sciendo

POLISH MARITIME RESEARCH 1 (117) 2023 Vol. 30; pp. 13-24
10.2478/pomr-2023-0002

NUMERICAL INVESTIGATION OF LENGTH TO BEAM RATIO EFFECTS ON SHIP RESISTANCE USING RANSE METHOD

Tat-Hien Le *
Nguyen Duy Anh
Ho Chi Minh City University of Technology (HCMUT), Vietnam
Vietnam National University Ho Chi Minh City, Vietnam
Tran Ngoc Tu
Vietnam Maritime University, VietNam
Nguyen Thi Ngoc Hoa
Ho Chi Minh City University of Transport, Vietnam
Vu Minh Ngoc
Vietnam Maritime University, VietNam

* Corresponding author: *hienlt@hcmut.edu.vn (Tat-Hien Le)*

ABSTRACT

The paper discusses the length to beam (L/B) ratio effects on ship resistance at three different Froude numbers using unsteady RANSE simulation. First, the JBC ship model was used as an initial hull form for verification and validation of predicted ship resistance results with measured data, and then the influence of the L/B ratio on ship resistance was carried out. Ship hull forms with different L/B ratios were produced from the initial one by using the Lackenby method. The numerical results obtained show the L/B ratio's effect on ship resistance. Increases of the L/B ratio led to gradual reduction of the total ship resistance and vice versa. Analysis of the changing of the resistance components indicates that the pressure resistance changes are considerably larger than the frictional one. Finally, the paper analyses the difference in the flow field around the hull of the ship with variation of the L/B ratio to fully understand the physical phenomenon in the change of ship resistance at different L/B parameters.

Keywords: Length-beam ratio, L/B, Resistance, hull form, RANSE

INTRODUCTION

A primary interest for ship owners and ship management is reducing fuel consumption and carbon emissions in marine traffic because they are related to both economic efficiency and the implementation of the requirements of the International Maritime Organization (IMO) on energy saving and emission reduction.

The first step in the ship design process is to determine the main dimensions of the ship, including the length, breadth, draft, and depth. Then the designers need to estimate the ship's displacement and select other basic ship design quantities and hull form characteristics. In that, the reasonable selection of the ship's main dimensions plays an important role because of their effects on the ship's hydrodynamic performance, ship stability, structural weight and construction cost, utilization of spaces, etc. [1, 2]. With respect to the ship performance, the L/B parameter is an important hydrodynamic parameter that plays a unique role in ship hydrodynamic design and minimizing ship resistance.

There are quite a few research works that deal with the influence of the L/B parameter on the resistance of the ship. Papanikolaou [1] used the Taylor–Gertler semi-empirical method for investigating the effects of the L/B ratio on ship resistance. In this study, the L/B ratios are changed in the range of ±10% while the ship's displacement, draft, and hull form coefficients are constant between variants. The results obtained show that the effect of the L/B parameter on ship

resistance is significant. When increasing the L/B ratio to 10%, the ship resistance reduces by 21%. However, as the L/B ratio is reduced to 10%, the ship resistance increases to 42% in comparison with the initial variant. Banawan and Ahmed [3] applied Computational Fluid Dynamics (CFD) for studying the influence of varying L/B parameters on ship resistance. In this study, the L/B ratio was changed in a range from -15% to +7.5%, while the displacement, B/T, block coefficient (CB) and longitudinal centre of buoyancy (LCB) were constant between variants. The results obtained indicate that as the L/B ratio increases the total ship resistance decreases and vice versa. These studies play an essential role in further research about the effect of the L/B parameter on ship resistance. Nevertheless, the research reviewed above still lacks any discussion of the change in the flow field around the hull of the ship at different L/B ratios to explain the physical phenomenon.

The key to selecting the optimum L/B ratio with respect to minimizing ship resistance is to evaluate the ship resistance accurately and efficiently. Nowadays, there are two common methods to predict the ship resistance, which are a model test in a towing tank and numerical simulation. The model test method still provides the most accurate results but is both costly and time-consuming with respect to both manufacturing the physical model and the experiment itself. Thus, this method is generally impractical for the initial ship design process. The latter method is more efficient and convenient than the model test method in analysing the flow field, which allows designers to develop or improve their design for hydrodynamics optimization studies [4, 5]. In recent years, for numerical simulation, the Reynolds Averaged Navier–Stokes Equations (RANSE) approach has been widely used for ship hydrodynamic prediction in general [6-8] and ship resistance prediction in particular, due to sufficient accuracy and efficient computation for engineering purposes [9-18]. Therefore, this research will focus on studying the influence of the L/B parameter on ship resistance by using the RANSE method. Evaluation of the change in the flow field around the ship hull with variation of the L/B parameter is conducted to fully understand the physical phenomenon of changing ship resistance at different L/B parameters.

NUMERICAL SIMULATION

HULL GEOMETRY

In this study the JAPAN Bulk Carrier (JBC) was used as an initial hull form for verification and validation study and for producing a new hull form with different L/B ratios. The computation was conducted at model scale λ=40. The hull geometry and principal particulars of the JBC model are presented in Fig. 1 and Table 1, respectively. The data for the ship resistance test are available in [19].

Tab. 1. Principal particulars of the JBC model

Description		Value
Length between perpendiculars	L_{pp} [m]	7.00
Breadth	B [m]	1.125
Draft	T [m]	0.4125
Block coefficient	CB [-]	0.858
Prismatic coefficient	CP [-]	0.860
Midship section area coefficient	CM [-]	0.998
Volume displacement	∇ [m³]	2.7870
Wetted surface	S [m²]	12.22

NUMERICAL SETUP

The Star-CCM+ (Version 15.02.007-R8) CFD modelling software was utilized in the present study to perform the computations. The setting was conducted corresponding to the setup in the towing tank of the National Maritime Research Institute (NMRI), Japan [20], as follows:

- For environment condition: calm water condition; water density ρ=998.2 kg/m³; kinematic viscosity of water ν =1.1070x10⁻⁶ m²/s.
- For test case: ship without appendages; volume displacement 2.787m³; the ship hull is free to heave and trim.

For ship resistance simulation, because the ship hull is symmetric, to save time, the simulation is carried out on only half of the hull. The computational domain sizes are set following the ITTC practical guidelines for ship CFD application [21]. The inlet and outlet boundaries are located two ship lengths upstream from the ship bow and three ship lengths downstream from the ship stern, respectively. The lateral boundary is placed at 2.5 ship lengths away from the ship's symmetry plane. The bottom and top of the computation domain are set at 2.5 and 1.25 ship lengths away from the free surface, respectively. The boundary conditions are specified as follows: at the inlet boundary, the velocity (for both water and air) is specified by the velocity of the hull; at the outlet, hydrostatic pressure is used; and the symmetry condition is applied at the central plane of the hull and lateral wall. The ship hull body is considered as a rigid body, so the no-slip wall condition was specified for the hull surfaces.

The numerical simulation was conducted by using three-dimensional incompressible viscous unsteady RANSE. The

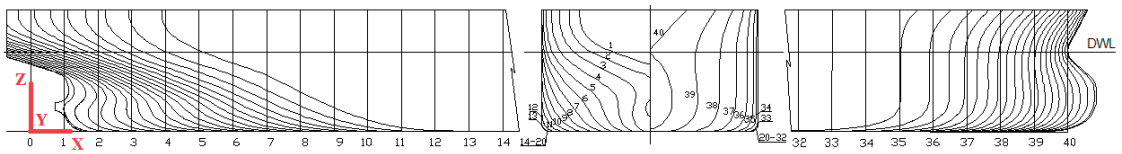

Fig. 1. Hull geometry of the JBC

SST K-ω turbulence model is used in the present paper as this model has been shown to be able to give accurate predictions of the ship hydrodynamics [22]. The volume of fluid (VOF) method was used to resolve the interfaces between water and air at the free surface. The motion of the ship with two degrees of freedom (heaving and pitching motion) is captured during the computation by using the dynamic fluid body interaction (DFBI) equilibrium option. All Y+ wall treatment was used for the simulation [23].

In this paper, hexahedral mesh was applied for the numerical simulation. The mesh near the free surface was refined to capture exactly the Kelvin wave. To avoid using a fine grid, which is not necessary (far from the ship in all directions), volumetric controls were created to refine the importance zone (around the bow and stern of the ship). Prism layer meshes were used for the boundary layer to capture exactly the flow behaviour near the walls, and the thickness of the first cell of the prism layer near the wall was set in order to keep an average Y+ value on the submerged part of the hull of approximately 60 (see Fig. 2), which was found in the past to produce the best solutions [24]. The resulting structure of the grid around the hull and on the free surface is illustrated in Fig. 3.

Fig. 2. Y+ value on hull surface

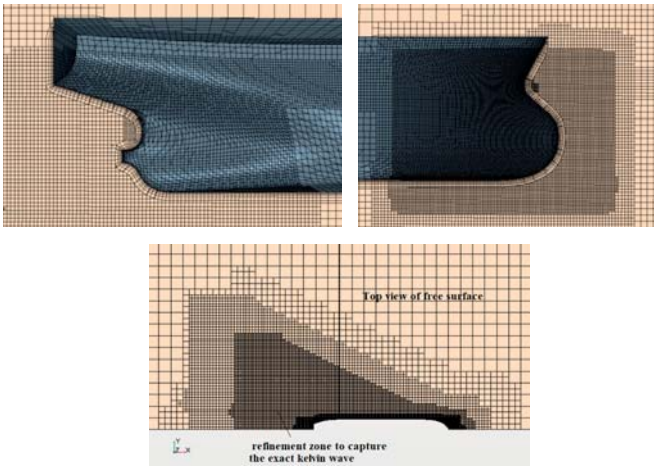

Fig. 3. Structure of grid around the hull and on the free surface

UNCERTAINTY ANALYSIS

In this study, the ITTC procedures were used for the uncertainty analysis in CFD. According to these procedures [25], the numerical uncertainty is mainly composed of grid, time step and iterative uncertainties. Here unsteady flow is implemented for the numerical simulation with the time step defined by Eq. (1), so the time step uncertainty (U_T) is neglected in this study. The iterative uncertainty (U_I) is also neglected due to the fact that the iterative errors are much smaller than the relative change of the calculation parameters with the mesh size. Therefore, the numerical uncertainty (U_{SN}) is equal to the grid uncertainty (U_G) [26]. The validation uncertainty is calculated according to $U_V = \sqrt{U_G^2 + U_D^2}$, where UD is the uncertainty of the model test. The experimental uncertainty was not provided in the reference study; therefore, the validation uncertainty was assumed as $U_v \cong U_G$.

$$\Delta t = 0.005 \sim 0.01 L/U \tag{1}$$

where U is the speed of the ship, (m/s), and L is a characteristic length value, (m).

The grid uncertainty is conducted with three grids, including coarse, medium, and fine grids corresponding to the cell numbers of 0.725, 1.59 and 3.35 million, respectively. The solution changes between two obtained simulation results such as fine-medium (ε_{21}) and medium-coarse (ε_{32}), and the convergence ratio (R), order of accuracy (p_i), the error (δ_{RE}), the correction factor (C_i) and the uncertainty for the uncorrected (U_i) approach are defined as follows for the case of 0<R<1 (monotonic convergence condition):

$$R = \frac{\varepsilon_{21}}{\varepsilon_{32}} \tag{2}$$

$$p = \frac{\ln(\varepsilon_{32}/\varepsilon_{21})}{\ln(r_i)} \tag{3}$$

$$\delta_{RE} = \frac{\varepsilon_{21}}{r_i^{p_i} - 1} \tag{4}$$

$$C_i = \frac{r_i^{p_i} - 1}{r_i^{p_{iest}} - 1} \tag{5}$$

$$U_i = \begin{cases} [9.6(1-C_i)^2 + 1.1]\left|\delta_{RE_{i,1}}\right|, & |1-C_i| < 0.125 \\ [2|1-C_i| + 1]\left|\delta_{RE_{i,1}}\right|, & |1-C_i| \geq 0.125 \end{cases} \tag{6}$$

The results of the grid uncertainty analysis and the comparison of the simulation results with the experimental data are described in Table 2 and Table 3, respectively.

Tab. 2. Result of uncertainty analysis based on the mesh dependency

Description		Value
Total resistance [N]	S_1 (fine)	35.580
	S_2 (mid)	35.790
	S_3 (coarse)	36.100
Refinement ratio	r_G	1.414
Convergence ratio	R_G	0.677
Order of accuracy	P_G	1.124
Error	δ_{RE}	0.441
Correction factor	C_G	0.476
Uncorrected uncertainty	U_G	0.903
Validation uncertainty	U_V	0.903

Table 3. Comparison of numerical obtained results with measured data

Parameter	Exp. data (D) [20]	CFD data (S)	
		Medium mesh	Fine mesh
Ship resistance [N]	36.60	35.79	35.58
Error E=D-S	/	0.57	0.78
Deviation [%]	/	1.57	2.18

It can be seen from Table 3 that the predicted total resistance agrees well with the experimental data, with deviations of 1.57% and 2.18% corresponding to medium and fine mesh, respectively. The validation of the present numerical simulations is achieved because the values of error E are smaller than the validation uncertainty U_V. Therefore, the medium mesh is used in further studies.

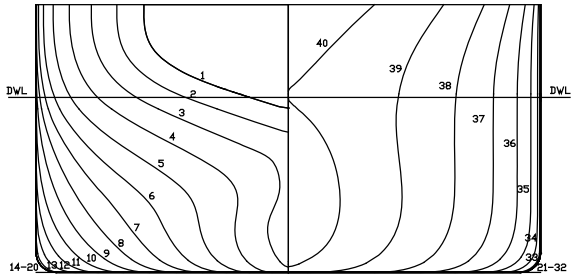

a) Variant No1 (L/B=5.717)

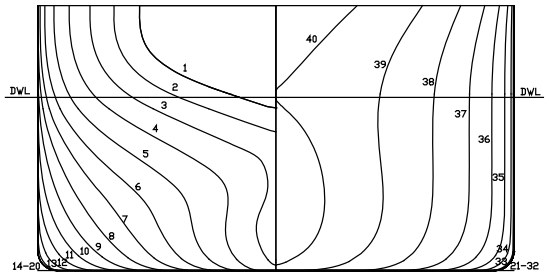

b) Variant No2 (L/B=6.020)

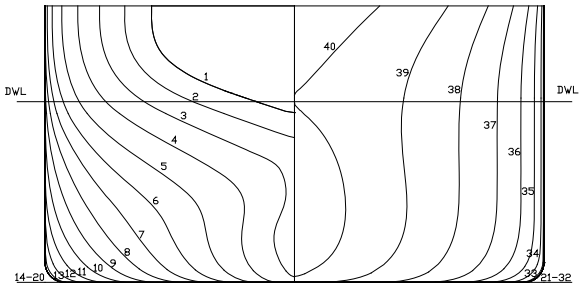

c) Variant No3 (L/B=6.333)

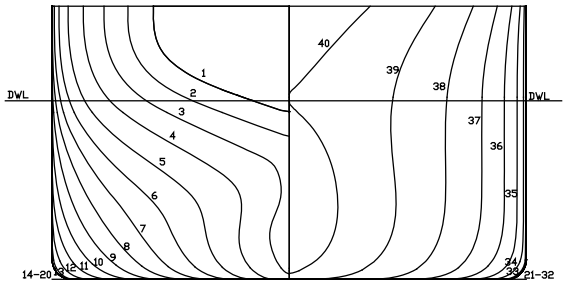

d) Variant No 4 (L/B=6.651)

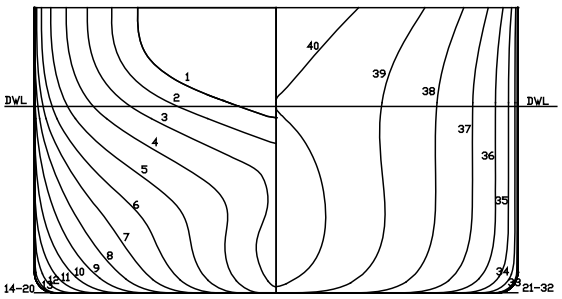

e) Variant No 5 (L/B=6.985)

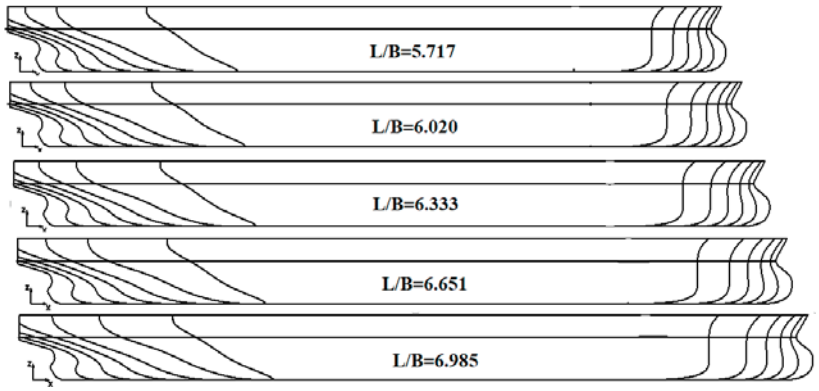

Fig. 4. The ship hull forms with modified L/B ratio

EFFECT OF L/B RATIO ON SHIP RESISTANCE AT DIFFERENT SHIP SPEEDS

CASE STUDIES

To investigate the influence of the L/B ratio on the resistance of the ship, CFD simulations are executed for the ship model with variation of the length to beam ratios. The hull model is generated while keeping the volume displacement, ship draft, block, prismatic, midship section area and waterplane area coefficients, etc., constant and varying only the L/B ratio by using the MAXSURF modeller's parametric transformation tool based on the Lackenby method. This method is a hull variation technique developed by H. Lackenby [27, 28].

In this study, five different L/B ratios are investigated with the length of the waterline and ship breadth changing in the range of ±5.0% with a step of ±2.5%. The main ship dimensions with variation of the L/B ratio are shown in Table 4. The ship hull forms with the modified L/B ratios are given in Fig. 4.

The computations were conducted at the design draft T=0.4125 with three Froude numbers, 0.122, 0.142 and 0.162.

Tab. 4. The main ship dimensions with variation of L/B ratio

Variant numbers	**1**	**2**	**3** (initial)	**4**	**5**
Length of waterline [m]	6.769	6.947	7.125	7.303	7.481
Breadth [m]	1.184	1.154	1.125	1.098	1.071
Draft [m]	0.4125				
Volume displacement [m^3]	2.787				
Midship section area coefficient [-]	0.998				
Waterplane area coefficient [-]	0.889				
Block coefficient [-]	0.858				
Prismatic coefficient [-]	0.86				
Wetted surface [m^2]	11.968	12.087	12.220	12.328	12.45
LCB from AP [m]	3.494	3.586	3.678	3.770	3.862
L/B ratio [-]	5.717	6.020	6.333	6.651	6.985

RESULTS AND DISCUSSION

The results of changes of the total ship resistance and their components as a function of the L/B ratio in comparison with the initial variant at three ship speeds are summarized in Table 5 and Figs. 5–7. The form of the relative change of resistance of the ship is given as follows:

$$\Delta R,\ \% = \frac{\left(\mathrm{R}_{\mathrm{var}} - R_0\right)}{R_0} \times .100\% \qquad (7)$$

where: R_0 – resistance at the initial variant; R_{var} – resistance of different variants of L/B ratio.

Tab. 5. Relative change of ship resistance as a function of L/B ratio in comparison with initial variant

L/B variant	**CFD computation**					
	R_T [N]	R_F [N]	R_P [N]	ΔDR_T [%]	ΔDR_F [%]	ΔDR_P [%]
Case study 1 (Draft T=0.4125, Fr=0.122)						
5.717	27.28	19.62	7.66	4.59	-0.71	21.13
6.020	26.63	19.69	6.94	2.09	-0.35	9.74
6.333	**26.084**	**19.76**	**6.32**	**0.00**	**0.00**	**0.00**
6.651	25.68	19.86	5.82	-1.55	0.51	-7.97
6.985	25.35	19.98	5.37	-2.81	1.11	-15.09
Case study 2 (Draft T=0.4125, Fr=0.142)						
5.717	37.59	26.4	11.19	5.03	-0.86	22.16
6.020	36.59	26.51	10.08	2.24	-0.45	10.04
6.333	**35.79**	**26.63**	**9.16**	**0.00**	**0.00**	**0.00**
6.651	35.17	26.8	8.37	-1.73	0.64	-8.62
6.985	34.61	26.95	7.66	-3.30	1.20	-16.38
Case study 3 (Draft T=0.4125, Fr=0.162)						
5.717	49.03	32.76	16.27	5.67	-1.03	22.33
6.020	47.576	32.92	14.66	2.53	-0.54	10.20
6.333	**46.4**	**33.1**	**13.30**	**0.00**	**0.00**	**0.00**
6.651	45.35	33.35	12.00	-2.26	0.76	-9.77
6.985	44.57	33.57	11.00	-3.94	1.42	-17.29

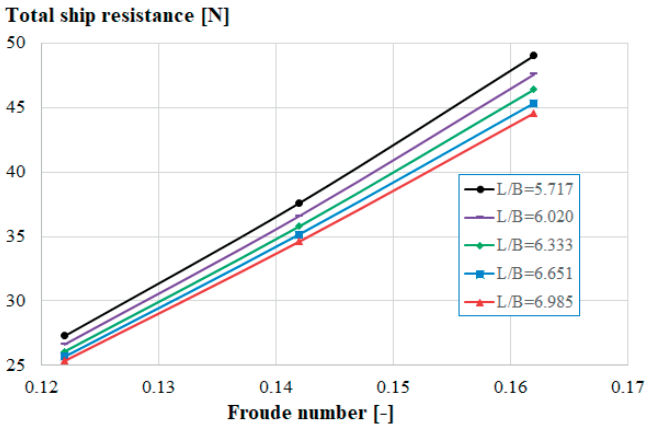

Fig. 5. Results of changes in total ship resistance with L/B variation at different Froude numbers

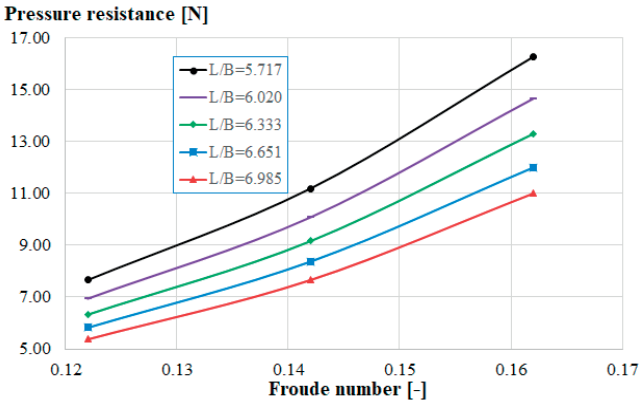

Fig. 6. Results of changes in pressure resistance component with L/B variation at different Froude numbers

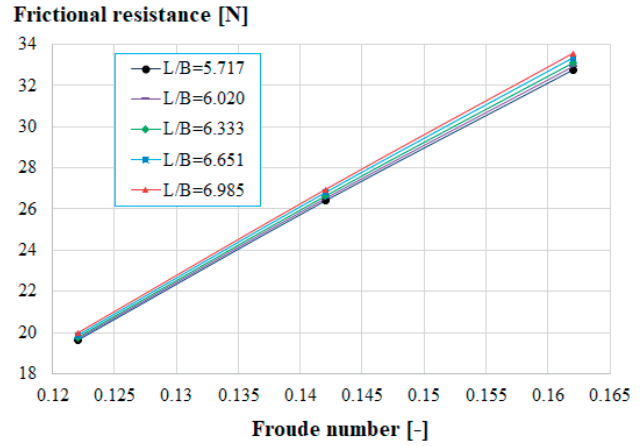

Fig. 7. Results of changes in frictional resistance component with L/B variation at different Froude numbers

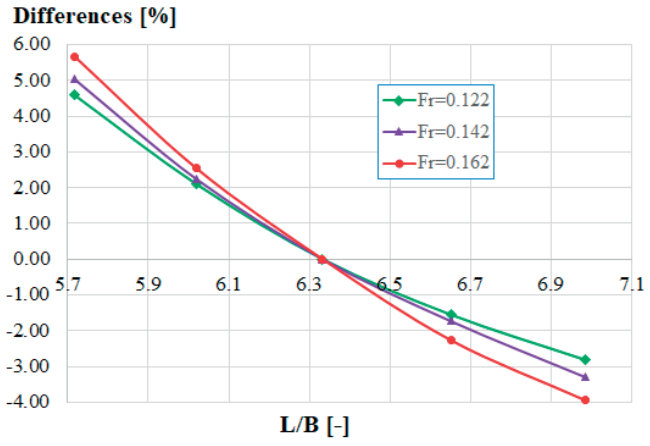

Fig. 8. Percentage changes of total resistance in comparison with initial L/B variant at different Froude numbers

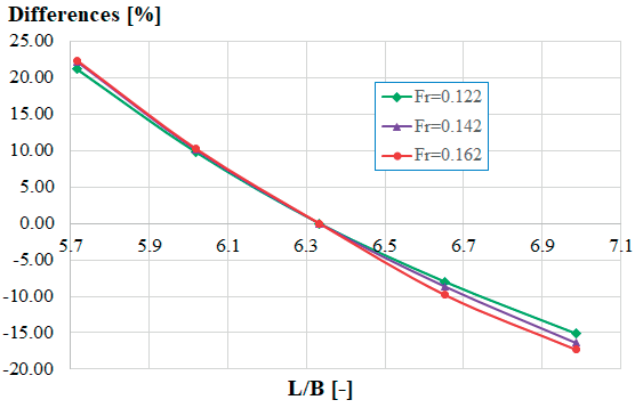

Fig. 9. Percentage changes of pressure resistance in comparison with initial L/B variant at different Froude numbers

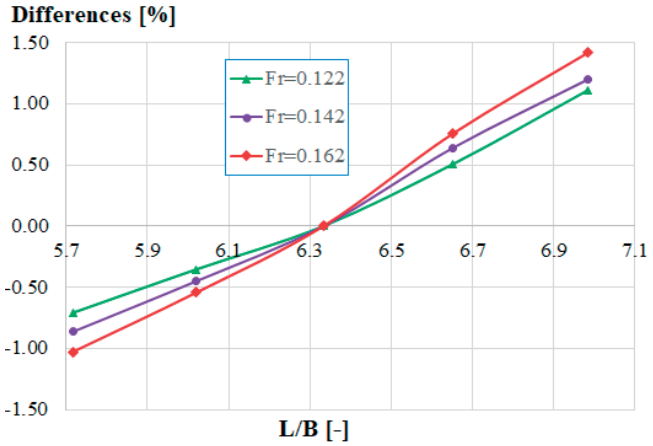

Fig. 10. Percentage changes of frictional resistance in comparison with initial L/B variant at different Froude numbers

Based on the numerical results obtained for the cases of the vessel analysed in Table 5, Figs. 5 – 10, it can be observed that:

- Generally, the L/B ratio has an effect on ship resistance. Increasing the L/B ratio led to a gradual reduction of the total ship resistance and vice versa. The level of change in the total ship resistance depends on the ship speed. Increasing the ship speed leads to an increase in the level of change in the total ship resistance, but not by much (see Figs. 5 and 8). For example, at Fr=0.122, the relative change of total ship resistance between variant L/B=5.717 and the initial variant (L/B=6.333) is +4.59%, while at Fr=0.142 and 0.162 this relative change increases to 5.03% and 5.67%, respectively.
- The changes in the level of the pressure resistance component corresponding to variation of the L/B ratio are significantly larger than those of the frictional resistance component. For example, at Froude number 0.142, the pressure resistance component changes from +22.16% to -16.38%, while the frictional resistance component changes only from -0.86 to +1.20% in comparison with the initial L/B variant when changing the L/B ratio in the range from 5.717 to 6.985, respectively (see Figs. 9 and 10).

– The changing tendency of the pressure resistance component is the same as the total ship resistance at the three different ship speeds. The pressure resistance component reduces monotonically when the L/B ratio increases and the level of change depends on the ship speed, but not greatly.
– The changing trend in the frictional resistance component is opposite to that of the pressure resistance component. The frictional resistance component monotonically increases when the L/B ratio increases and the level of change is not large, around -0.5% to 1.42% for all three case studies, and does not depend greatly on the ship speed.

The trend and level of change in the ship resistance components when varying the L/B ratio can be partly explained by the changes of flow around the ship.

The variation of the pressure resistance component can be partly explained by the difference in the wave pattern and in the dynamic pressure distribution on the hull surface at different L/B ratios (see Figs. 11–19). As can be observed in Figs. 11, 12 and 13, the wave cut along the y/L=0 plane (z represents the height of the free surface) changes monotonically and is the same at different ship speeds. At the position of the first wave trough near the ship bow (at X/L=0.9) and at the stern region (at X/L=0.2), the height of the wave trough reduces gradually when increasing the L/B ratio. At the location X/L=0.9 along the ship length, the biggest and smallest height of wave trough are observed at variants L/B=5.717 and L/B=6.985, respectively. The height of the wave trough for variant L/B=5.717 is approximately 1.5 times greater than for variant L/B=6.985 at different ship speeds. At the location X/L=0.2, the height of the wave trough for variant L/B=5.717 is approximately 1.2, 1.5 and 2.5 times bigger than for variant L/B=6.985 at Froude numbers of 0.122, 0.142, and 0.162, respectively; consequently, it is one of the causes of the increase in the pressure resistance component when reducing the L/B ratio.

The resulting difference in the dynamic pressure pattern distribution on the ship surface with variations of the L/B ratio (shown in Fig. 14) also provides some explanations for the resistance changes. It can be seen from Figs. 15, 16 and 17 that the dynamic pressure at Z=0.0075 m changes monotonically and similarly with different ship speeds. At the stern (locations from X/L= 0.05 to 0.3 along the ship length) and bow regions (locations from X/L= 0.8 to 0.95 along the ship length), the negative dynamic pressure increases gradually when reducing the L/B ratio. At locations from X/L=0.3 to X/L=0.8 along the ship length, the dynamic pressure has approximately the same value. At different Z locations, the changing tendency of the dynamic pressure is the same at Z=0.0075 m. For example, Figs. 18 and 19 illustrate the comparison of dynamic pressure for different variants of the L/B ratio at Z=0.3125 m and Z=0.1125 m, respectively, with Fr=0.142. It can be observed that the pattern of dynamic pressure has clearly similar changing trends in comparison with those obtained at Z=0.0075 m; consequently, it causes an increase of the pressure resistance component when reducing the L/B ratio.

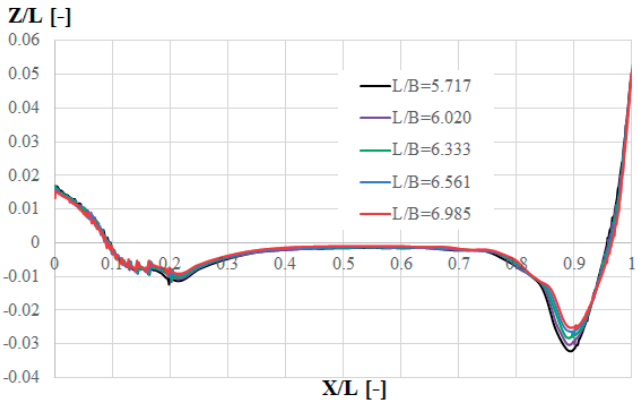

Fig. 11. Comparison of the wave profile at y/L=0 for different L/B variants at Fr= 0.122

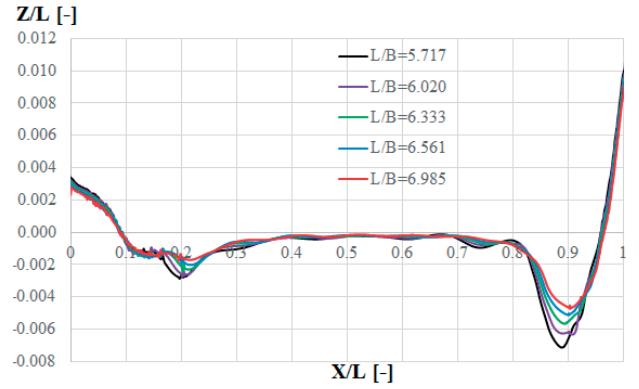

Fig. 12. Comparison of the wave profile at y/L=0 for different L/B variants at Fr= 0.142

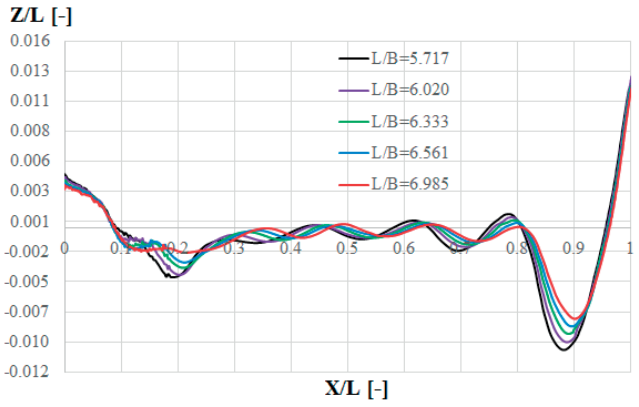

Fig. 13. Comparison of the wave profile at y/L=0 for different L/B variants at Fr= 0.162

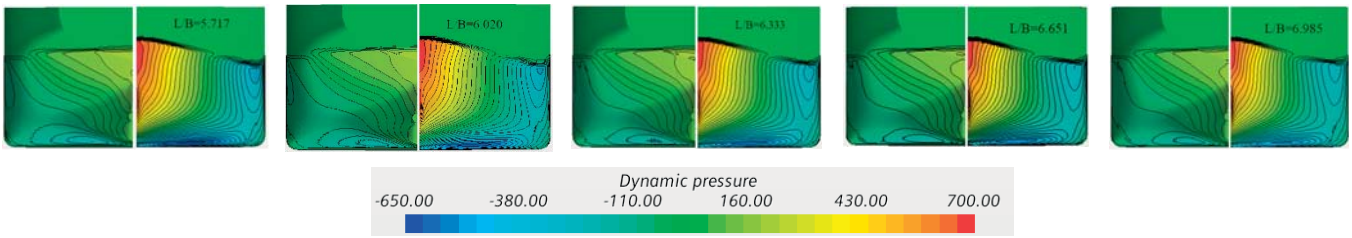

Fig. 14. Comparison of dynamic pressure distribution on the ship surface for different L/B variants at Fr= 0.142

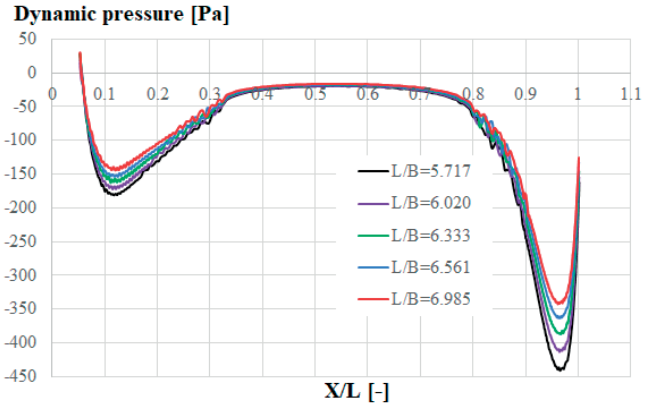

Fig. 15. Comparison of dynamic pressure for different L/B variants at Z=0.0075 m with Fr=0.122

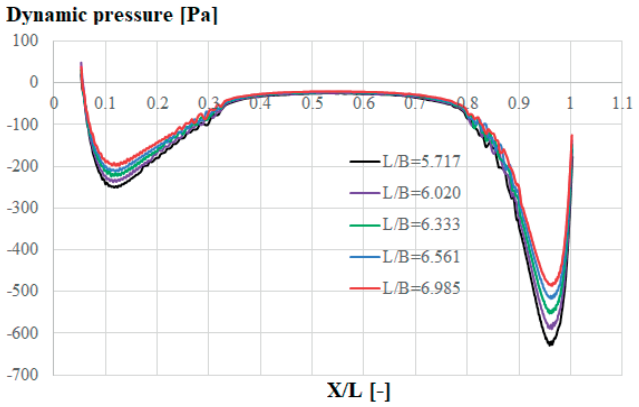

Fig. 16. Comparison of dynamic pressure for different L/B variants at Z=0.0075 m with Fr=0.142

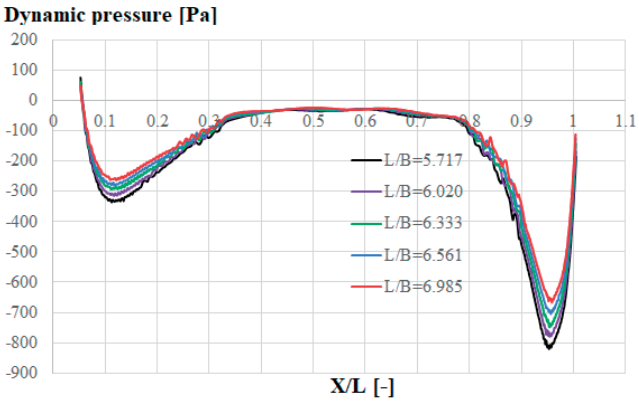

Fig. 17. Comparison of dynamic pressure for different L/B variants at Z=0.0075 m with Fr=0.162

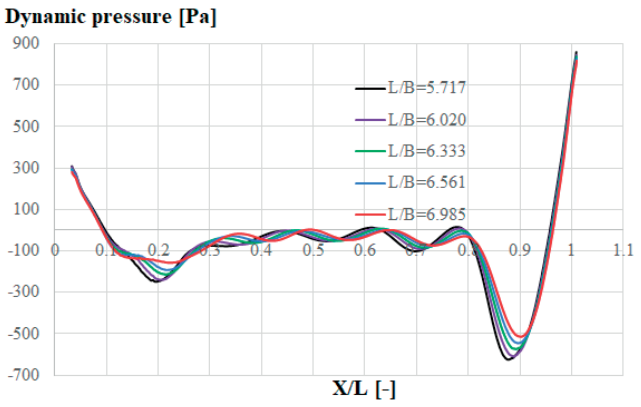

Fig. 18. Comparison of dynamic pressure for different L/B variants at Z=0.3125 m with Fr=0.142

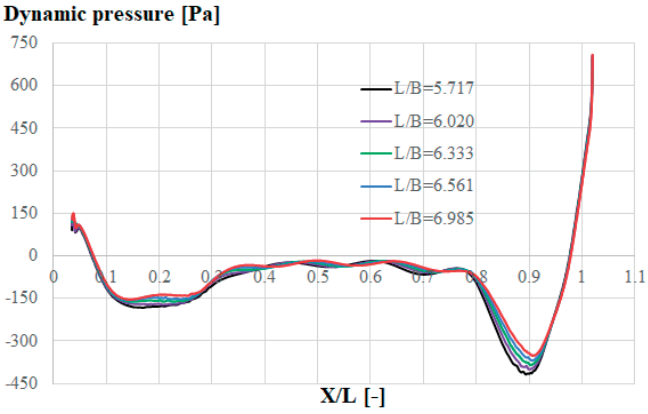

Fig. 19. Comparison of dynamic pressure for different L/B variants at Z=0.1125 m with Fr=0.142

The change in the frictional resistance component can be explained by the variation of the wetted surface area and by the difference in wall shear stress distribution at different variants of L/B (see Table 6 and Fig. 20, respectively), in which the wetted surface area is one of the primary variables affecting this resistance component [29].

Tab. 6. Relative change of wetted surface area as a function of L/B ratio in comparison with initial variant

L/B ratio	5.716	6.020	6.333	6.651	6.985
Wetted surface, S [m^2]	11.968	12.087	12.220	12.328	12.450
Relative change, [%]	-2.06	-1.09	0.00	+0.88	+1.88

$$R_F = C_F \frac{1}{2} \rho V^2 S \quad (8)$$

where C_F – the frictional resistance coefficient, ρ – water density, V - ship speed, S – wetted surface area.

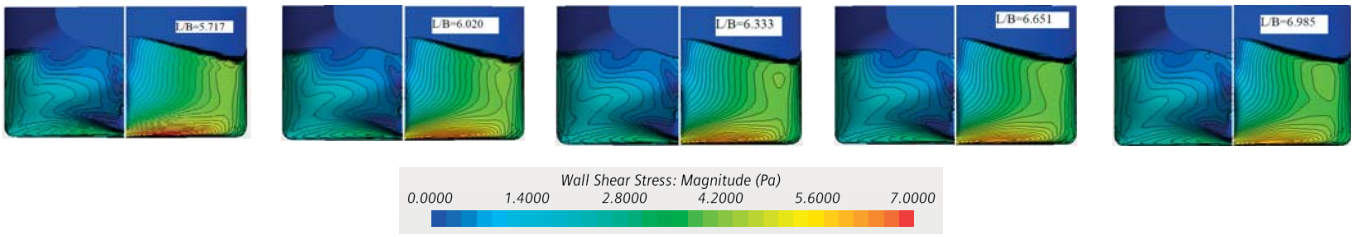

Fig. 20. Comparison of wall shear stress distribution on the ship surface for different L/B variants at Fr= 0.142

As can be seen in Table 6, increase of the L/B ratio leads to a monotonic increase in the wetted surface area, because of the increasing frictional resistance component. Here, the changes in this resistance component resulting from changes of the wetted surface itself are of the same order due to proportionality (see Eq. 8). This means that, if neglecting the changes in the frictional resistance coefficient, this resistance component changes from -2.06% to +1.88% in comparison with the initial L/B variant for L/B ratios changing in the range from 5.717 to 6.985, respectively. However, the level of change in the frictional resistance is less than this value. For example, at Fr=0.162, this resistance component only changes from -1.03% to 1.42% in comparison with the initial variant L/B for L/B ratios changing in the range from 5.717 to 6.985, respectively. This can be explained by the difference in the wall shear stress distribution on the hull surface with variations of the L/B ratio (see Fig. 20). It can be seen from Figs. 21, 22 and 23 that the wall shear stress at Z=0.0075 m changes monotonically and similarly with different ship speeds. At the stern (locations from X/L= 0.05 to 0.3 along the ship length) and bow regions (locations from X/L= 0.8 to 0.95 along the ship length), the wall shear stress reduces gradually when increasing the L/B ratio. At locations from X/L=0.3 to X/L=0.8 along the ship length, the wall shear stress has approximately the same value. At different Z locations, the changing tendency of the wall shear stress is the same at Z=0.0075 m. For example, Figs. 24 and 25 present the comparison of the wall shear stress for different variants of the L/B ratio at Z=0.1125 0 and Z=0.3125 m, respectively, with Fr=0.122. It can be observed that the wall shear stress has clearly similar changing trends in comparison with those obtained at Z=0.0075 m; consequently, this causes the frictional resistance coefficient to increase when reducing the L/B ratio. So finally, in the range of change in the L/B ratio, the level of change in the frictional resistance is less than the level of change in the wetted surface area.

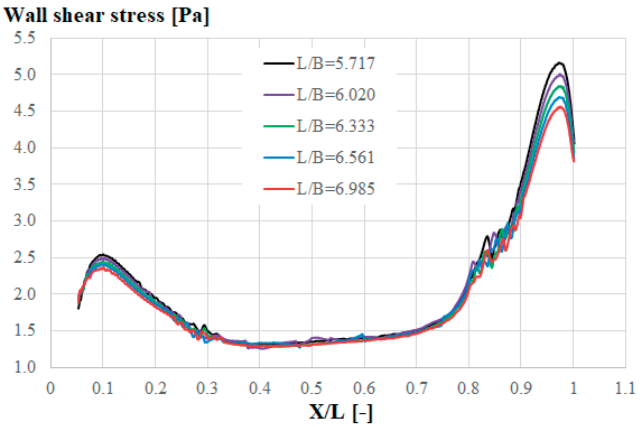

Fig. 21. Comparison of wall shear stress for different L/B variants at Z=0.0075 m with Fr=0.122

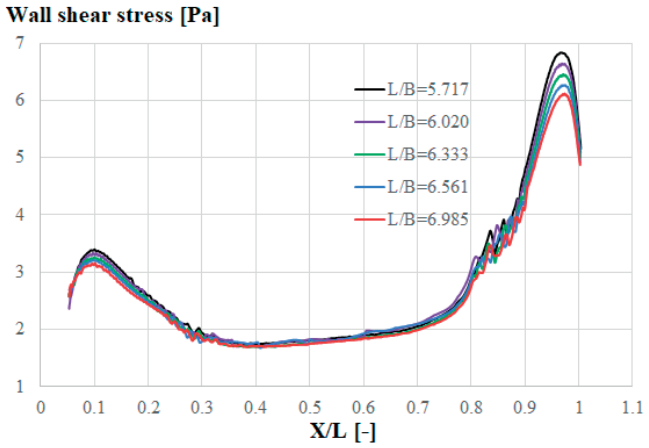

Fig. 22. Comparison of wall shear stress for different L/B variants at Z=0.0075 m with Fr=0.142

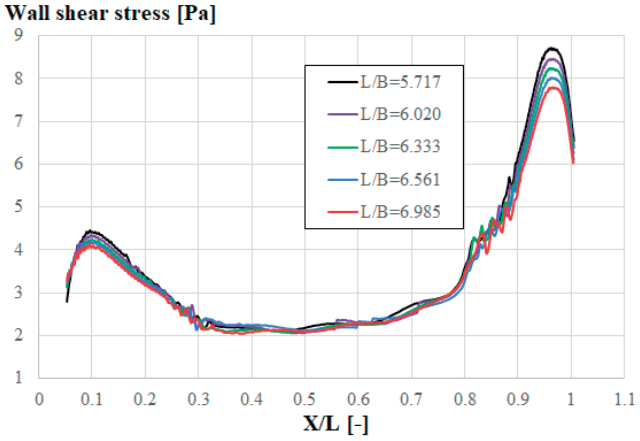

Fig. 23. Comparison of wall shear stress for different L/B variants at Z=0.0075 m with Fr=0.162

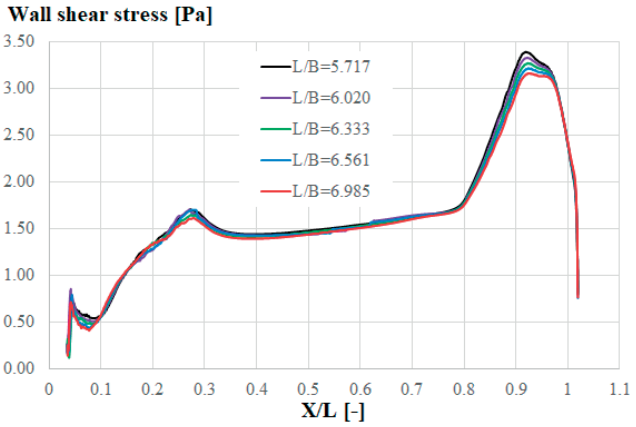

Fig. 24. Comparison of wall shear stress for different L/B variants at Z=0.1125 m with Fr=0.122

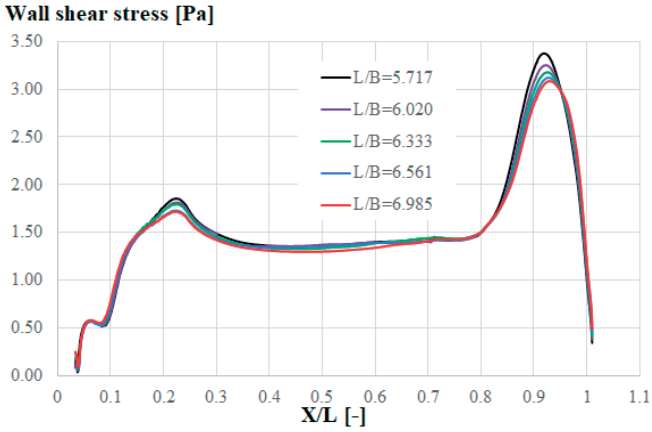

Fig. 25. Comparison of wall shear stress for different L/B variants at Z=0.3125 m with Fr=0.122

CONCLUSIONS

In this paper, the RANSE method has been used to study the influence of the length-beam ratio on ship resistance at model scale and at different ship speeds. To investigate this effect, five case studies with variation of the L/B ratio were carried out. The following conclusions can be drawn:

- There is good agreement between the numerical results obtained and the measured data, with a deviation of less than 2.0%. This shows the capability of CFD in the application of RANSE for ship hull form optimization.

– The total ship resistance changes with variation of the L/B ratio. Increasing the L/B ratio led to a gradual reduction of the total ship resistance and vice versa. The impact level of the L/B ratio depends on the ship speed and hull form, so estimating reasonable L/B ratios is therefore a dynamic process. In the case of the vessel analysed, the L/B ratio increases from 6.333 (initial variant) to 6.985, leading to a decrease of the total ship resistance by 2.81%, 3.30%, and 3.94% at the Froude numbers 0.122, 0.142, and 0.162, respectively.

– The resistance components analysis indicates that the change of the pressure resistance component corresponding to variation of the L/B ratio is considerably greater than for the frictional resistance component. In particular, when the L/B ratio increases from 5.717 to 6.985, the pressure resistance component changes from +22.16% to -16.38%, while the frictional resistance component changes only from -0.86% to +1.20% in comparison with the initial variant L/B at Froude number 0.142, respectively.

– Analysis of the change in the flow field around the ship hull with variation of L/B provides a full explanation of the physical phenomenon of changing ship resistance when changing the L/B ratio.

– Investigation of the effect of the L/B ratio on ship resistance is essential during the initial design stage. It helps the designer to make a suitable compromise between the different hull form parameters to acquire a good design that fulfills the different design requirements.

ACKNOWLEDGEMENT

We acknowledge the support of time and facilities from Ho Chi Minh City University of Technology (HCMUT), Vietnam National University Ho Chi Minh City (VNU-HCM) for this study.

REFERENCES

1. A. Papanikolaou, 'Ship design: Methodologies of preliminary design', Springer, 2014. https://doi.org/10.1007/978-94-017-8751-2

2. O. Kanifolskyi, 'General Strength, Energy Efficiency (EEDI), and Energy Wave Criterion (EWC) of Deadrise Hulls for

Transitional Mode,' *Polish Maritime Research*, vol. 29, no. 3, pp. 4-10, 2022. https://doi.org/10.2478/pomr-2022-0021

3. A. A. Banawan, and Y. M. Ahmed, 'Use of computational fluid dynamics for the calculation of ship resistance, and its variation with the ship hull form parameters,' *Alexandria Engineering Journal*, vol. 45, no. 1, pp. 47-56, 2006

4. M. Kraskowski, 'CFD Optimisation of the Longitudinal Volume Distribution of a Ship's Hull by Constrained Transformation of the Sectional Area Curve,' *Polish Maritime Research*, vol. 29, no. 3, pp. 11-20, 2022. https://doi.org/10.2478/pomr-2022-0022

5. D. D. Luu et al., 'Numerical Study on the Influence of Longitudinal Position of Centre of Buoyancy on Ship Resistance Using RANSE Method,' *Naval Engineers Journal*, vol. 132, no. 4, pp. 151-160, 2020.

6. T. N. Tu et al., 'Numerical prediction of propeller-hull interaction characteristics using RANS method,' *Polish Maritime Research*, vol. 26, no. 2, pp. 163-172, 2019. https://doi.org/10.2478/pomr-2019-0036

7. Y. Zhang et al., 'Feasibility study of RANS in predicting propeller cavitation in behind-hull conditions,' *Polish Maritime Research*, vol. 27, no. 4, pp. 26-35, 2020. https://doi.org/10.2478/pomr-2020-0063

8. H. Nouroozi, and H. Zeraatgar, 'Propeller hydrodynamic characteristics in oblique flow by unsteady RANSE solver,' *Polish Maritime Research*, vol. 27, no. 1, pp. 6-17, 2020. https://doi.org/10.2478/pomr-2020-0001

9. T. N. Tu et al.,' Numerical Study on the Influence of Trim on Ship Resistance in Trim Optimization Process,' *Naval Engineers Journal*, vol. 130, no. 4, pp. 133-142, 2018.

10. N. Sakamoto et al., 'Estimation of Resistance and Self-Propulsion Characteristics for Low L/B Twin-Skeg Container Ship by a High-Fidelity RANS Solver,' *Journal of Ship Research*, vol. 57, no. 01, pp. 24-41, 2013. https://doi.org/10.5957/jsr.2013.57.1.24

11. T. Q. Chuan et al., 'Numerical Study of Effect of Trim on Performance of 12500DWT Cargo Ship Using RANSE Method,' *Polish Maritime Research*, vol. 29, no. 1, pp. 3-12, 2022. https://doi.org/10.2478/pomr-2022-0001

12. J. Choi et al., 'Resistance and propulsion characteristics of various commercial ships based on CFD results,' *Ocean Engineering*, vol. 37, no. 7, pp. 549-566, 2010. https://doi.org/10.1016/j.oceaneng.2010.02.007

13. S. Bhushan et al., 'Model-and full-scale URANS simulations of Athena resistance, powering, seakeeping, and 5415 maneuvering,' *Journal of Ship Research*, vol. 53, no. 4, pp. 179-198, 2009. https://doi.org/10.5957/jsr.2009.53.4.179

14. K.-W. Song et al., 'Experimental and numerical study on the scale effect of stern flap on ship resistance and flow field,' *Ships and Offshore Structures,* vol. 15, no. 9, pp. 981-997, 2020. https://doi.org/10.1080/17445302.2019.1697091

15. Y. K. Demirel, O. Turan, and A. Incecik, 'Predicting the effect of biofouling on ship resistance using CFD,' *Applied Ocean Research*, vol. 62, pp. 100-118, 2017. https://doi.org/10.1016/j.apor.2016.12.003

16. B. Guo, G. Deng, and S. Steen, 'Verification and validation of numerical calculation of ship resistance and flow field of a large tanker,' *Ships and Offshore Structures*, vol. 8, no 1, pp. 3-14, 2013. https://doi.org/10.1080/17445302.2012.669263

17. Y. Zhang et al., 'Feasibility study of RANS in predicting propeller cavitation in behind-hull conditions,' *Polish Maritime Research*, vol. 27, no. 4, pp. 26-35, 2020. https://doi.org/10.2478/pomr-2020-0063

18. N. T. N. Hoa et al., 'Numerical investigating the effect of water depth on ship resistance using RANS CFD method,' *Polish Maritime Research*, vol. 26, no. 3, pp. 56-64, 2019. https://doi.org/10.2478/pomr-2019-0046

19. https://t2015.nmri.go.jp/Instructions_JBC/instruction_JBC.html.

20. https://t2015.nmri.go.jp/Instructions_JBC/Case_1-1a.html.

21. ITTC 2011. Practical guidelines for ship CFD applications. In: Recommended Procedure and Guidelines, ITTC 7.5–03-02–03. Available from https://ittc.info/media/1357/75-03-02-03.pdf.

22. Z. Yong et al., 'Turbulence model investigations on the boundary layer flow with adverse pressure gradients,' *Journal of Marine Science*, vol. 14, no. 2, pp. 170-174, 2015. https://doi.org/10.1007/s11804-015-1303-0

23. T.-H. Le et al., 'Numerical investigation on the effect of trim on ship resistance by RANSE method,' *Applied Ocean Research*, vol. 111, p. 102642, 2021. https://doi.org/10.1016/j.apor.2021.102642

24. R. A. Repetto, *'Computation of Turbulent Free Surface Flows Around Ships and Floating Bodies'*. 2001: Arbeitsbereiche Schiffbau der Techn. Univ. Hamburg-Harburg.

25. ITTC – Recommended Procedures and Guidelines, 2017. Uncertainty Analysis in CFD Verification and Validation Methodology and Procedures. ITTC 7.5-03-01-01. Available from https://www.ittc.info/media/8153/75-03-01-01.pdf

26. F. Stern et al., 'Comprehensive approach to verification and validation of CFD simulations—part 1: methodology and procedures,' *Journal of Fluids Engineering,* vol. 123, no. 4, pp. 793-802, 2001. https://doi.org/10.1115/1.1412235

27. H. Lackenby, 'On the systematic geometrical variation of ship forms,' *Trans INA*, vol. 92, pp. 289-316, 1950.

28. M.-I. Roh, and K.-Y. Lee, *'*Computational ship design'. Springer, 2018. https://doi.org/10.1007/978-981-10-4885-2

29. A. F. Molland, S. R. Turnock, and D. A. Hudson, *'Ship resistance and propulsion*'. Cambridge University Press, 2017https://doi.org/10.1017/CBO9780511974113